

# Thermal conductivity of bulk $\text{In}_2\text{O}_3$ single crystals

Liangcai Xu<sup>1,2</sup>, Benoit Fauqué<sup>3</sup>, Zengwei Zhu<sup>2</sup>, Zbigniew Galazka<sup>4</sup>, Klaus Irmscher<sup>4</sup>, Kamran Behnia<sup>1</sup>

(1) *Laboratoire de Physique Et Etude des Matériaux (UPMC-CNRS), ESPCI Paris, PSL Research University, 75005 Paris, France*

(2) *Wuhan National High Magnetic Field Center and School of Physics, Huazhong University of Science and Technology, Wuhan 430074, China*

(3) *Collège de France,*

*11 place Marcelin Berthelot, 75005 Paris, France*

(4) *Leibniz-Institut für Kristallzuchtung, Max-Born-Str. 2, 12489 Berlin, Germany*

(Dated: December 22, 2024)

The transparent semiconductor  $\text{In}_2\text{O}_3$  is a technologically important material. It combines optical transparency in the visible frequency range and sizeable electric conductivity. We present a study of thermal conductivity of  $\text{In}_2\text{O}_3$  crystals and find that around 20 K, it peaks to a value as high as  $5,000 \text{ WK}^{-1}\text{m}^{-1}$ , comparable to the peak thermal conductivity in silicon and exceeded only by a handful of insulators. The amplitude of the peak drastically decreases in presence of a type of disorder, which does not simply correlate with the density of mobile electrons. Annealing enhances the ceiling of the phonon mean free path. Samples with the highest thermal conductivity are those annealed in the presence of hydrogen. Above 100 K, thermal conductivity becomes sample independent. In this intrinsic regime, dominated by phonon-phonon scattering, the magnitude of thermal diffusivity,  $D$  becomes comparable to many other oxides, and its temperature dependence evolves towards  $T^{-1}$ . The ratio of  $D$  to the square of sound velocity yields a scattering time which obeys the expected scaling with the Planckian time.

$\text{In}_2\text{O}_3$  is a technologically appealing wide-gap semiconductor (see [1] for a review). Its main polymorph crystallizes in a cubic bixbyite structure [2]. The cubic (primitive) unit cell of this structure contains 16 (8) molecules and 80 (40) atoms. Introducing Sn dopants turns this semiconducting solid to a transparent conductor known as indium-tin-oxide (ITO) [3]. Electrical transport properties of doped  $\text{In}_2\text{O}_3$  with the carrier density in the range of  $10^{18} - 10^{20} \text{ cm}^{-3}$  has documented a room-temperature mobility in the range carrier of  $\sim 100\text{-}200 \text{ cm}^2\text{V}^{-1}\text{s}^{-1}$ . The high transparency in the visible spectrum makes this system an established transparent conducting material.

Amorphous/granular indium oxide ( $\text{InO}_x$ ) has been the subject of an independent fundamental research activity focusing on a fascinating two-dimensional superconductor [4]. It is platform to study metal-anomalous metal-superconductor transition [5] and host to a number of remarkable low-temperature transport properties [6]. The connection between this two-dimensional electronic system and the superconducting ground state of crystalline doped thin films of  $\text{In}_2\text{O}_3$  [7] is yet to be clarified.

Only recently [8, 9], bulk single crystals of  $\text{In}_2\text{O}_3$  became available. Previous to the present study, thermal transport in indium oxide, except for a study of room-temperature thermal diffusivity in tin-doped polycrystalline thin films [10], was not explored. The direct growth of single crystals from the melt [9] have made this task now achievable.

In this paper, we present a study of temperature dependence of thermal conductivity in single crystals of  $\text{In}_2\text{O}_3$ . We find that the peak thermal conductivity in  $\text{In}_2\text{O}_3$  crystal can reach as high as  $5000 \text{ WK}^{-1}\text{m}^{-1}$ . In

few other solids, such as diamond [11, 12] and sapphire (crystalline  $\text{Al}_2\text{O}_3$ ) [13] this peak is exceeded in magnitude. Most oxides show a much more modest maximum thermal conductivity. We find that this peak is drastically reduced by disorder. However, the level of disorder is not simply set by dopant concentration and depends on annealing conditions. Samples annealed in the presence of hydrogen are those showing the highest thermal conductivity. Above 100 K, thermal conductivity,  $\kappa$  in all samples converge to a similar magnitude. In this intrinsic regime (governed by phonon-phonon scattering), the ratio of the thermal diffusivity to sound velocity respects a boundary observed recently for all insulating solids [14, 15]. A comparison with  $\text{Al}_2\text{O}_3$  is in agreement with a picture proposed recently to explain this boundary [16]. The proximity of this system with other oxides and ionic salts (in contrast to harmonic solids with diamond-like structure) may point to a threshold for emergence of quantum chaos [17] driven strong phonon-phonon coupling [18].

Bulk  $\text{In}_2\text{O}_3$  single crystals were grown with a novel crystal growth technique under the name Levitation-Assisted Self-Seeding Crystal Growth Method (LASS-CGM) as described in detail by Galazka *et al.*[19, 20] that enabled to obtain bulk single crystals up to 35 mm in diameter and 12 mm thick. The as-grown crystals were dark red or dark brown and highly conducting with the free electron concentration of  $1 - 4 \times 10^{18} \text{ cm}^{-3}$  and Hall electron mobility of  $130 - 170 \text{ cm}^2\text{V}^{-1}\text{s}^{-1}$  [19, 20]. Annealing in the presence of oxygen and hydrogen allowed tuning the free electron concentration between  $1 \times 10^{18}$  and  $6 \times 10^{19} \text{ cm}^{-3}$  and increase the room-temperature

TABLE I. **Samples:** The  $\text{In}_2\text{O}_3$  single crystals investigated by the present study.  $n$  and  $\rho$  refer to room temperature carrier concentration and resistivity.  $\kappa_{peak}$  refers to the peak thermal conductivity. All samples were cut to  $5 \times 3 \times 0.5 \text{ mm}^3$ . The orientations relate to the largest plane ( $5 \times 3 \text{ mm}^2$ ).

sample	Orientation	Annealing conditions	$n(10^{17} \text{ cm}^{-3})$	$\rho(\text{m}\Omega.\text{cm})$	$\kappa_{peak} (\text{WK}^{-1}\text{m}^{-1})$
#1	(111)	As-grown	12	17	100
#2	(111)	900°C, 40 h, air	2	95	300
#3	(001)	1000°C, 40 h, air	3	89	450
#4	(110)	1000°C, 40 h, $\text{O}_2$	12	45	480
#5	(111)	1000°C, 40 h, $\text{O}_2$ & 650°C, 10 h, $\text{H}_2$ (5%)+Ar	180	2.1	1200
#6	(111)	1000°C, 40 h, $\text{O}_2$ & 500°C, 10 h, $\text{H}_2$ (5%)+Ar	61	10	5000

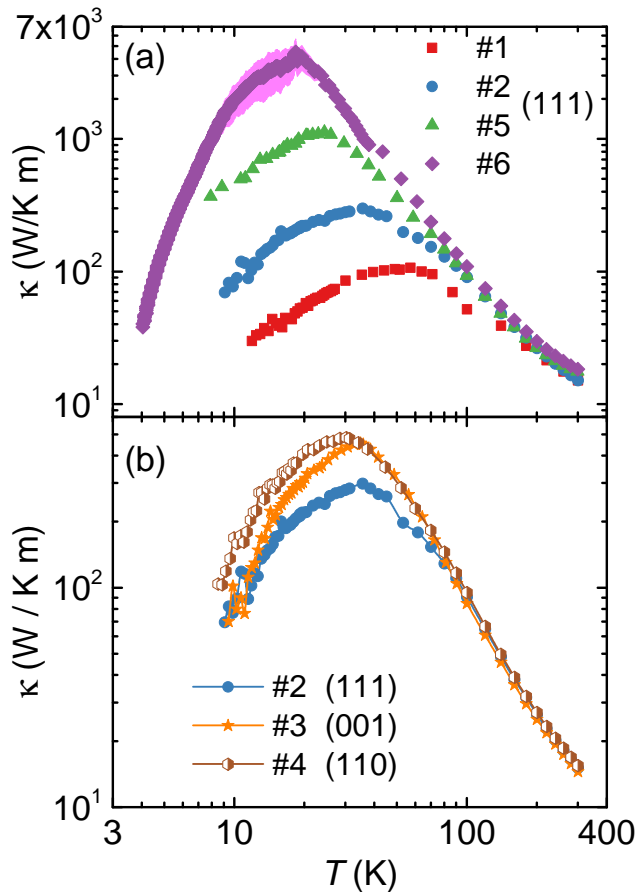


FIG. 1. **Thermal conductivity of  $\text{In}_2\text{O}_3$  and its sample dependence.** a) Thermal conductivity  $\kappa$  of four different samples of  $\text{In}_2\text{O}_3$ . Note the strong variation in the magnitude of maximum  $\kappa$  among the samples. Purple bars represent the margin of experimental reproducibility in repeated measurements on sample #6. Because of its large thermal conductance, the temperature difference caused by the application of the heat current was small leading to a larger experimental uncertainty. b) Comparison of thermal conductivity in three samples having different plane orientations. The heat current was always applied along the longest axis. No anisotropy is expected in this cubic system and the difference is due to different levels of disorder.

Hall electron mobility to  $200 \text{ cm}^2\text{V}^{-1}\text{s}^{-1}$ . Wafers fabricated from bulk single crystals were characterized by a very narrow rocking with the FWHM  $< 50$  arcsec. The dislocation etch pit density was found to be between  $5 \times 10^4$  and  $3 \times 10^5 \text{ cm}^{-2}$  [19, 20].

The single crystals studied in this work are listed in table I. We measured thermal conductivity in a steady-state configuration with one heater and two thermometers. Between 10 K and room temperature chromel-constantan thermocouples were employed with a set-up similar to the one used before [21]. In one sample(#6), this set of data was completed by measurements using Cernox chips between 2 K and 30 K. The two sets of data were found to be consistent at intermediate temperatures.

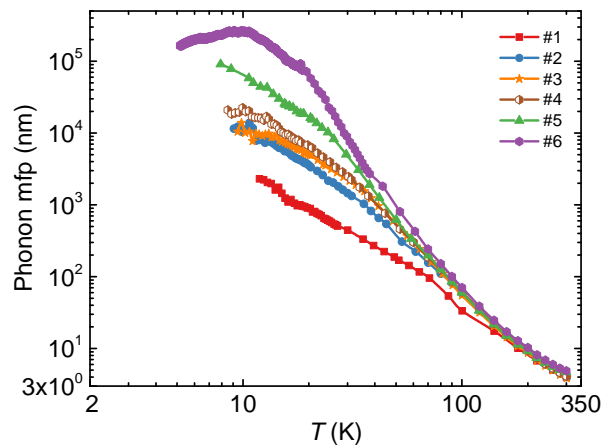


FIG. 2. **Phonon mean free path(mfp) in  $\text{In}_2\text{O}_3$ .**The phonon mean free path extracted from thermal conductivity, specific heat and the sound velocity. The electric resistivity and the carrier density of these samples are listed in table I. There is no visible correlation between the electronic properties and phonon mean free path. Note that in the best sample (#6), the mean free path approaches the sample thickness of 0.5 mm at low temperature.

Fig.1 presents our main result. Near room temperature, thermal conductivity increases with cooling and its magnitude is the same in all crystals studied. The room-temperature thermal conductivity of our bulk samples,  $\kappa(300 \text{ K}) = 15 \pm 2 \text{ WK}^{-1}\text{m}^{-1}$ , is comparable to

the value of  $13.1 \text{ WK}^{-1}\text{m}^{-1}$  obtained by the laser flash method [20] and three times larger than what was reported for thin films of ITO ( $\approx 5 \text{ WK}^{-1}\text{m}^{-1}$ ) [10]. In all samples,  $\kappa(T)$  shows a broad peak. The magnitude of this  $\kappa_{peak}$  is strongly sample dependent. It varies from  $100 \text{ WK}^{-1}\text{m}^{-1}$  in sample #1 to  $5000 \text{ WK}^{-1}\text{m}^{-1}$  in sample #6. The higher the  $\kappa_{peak}$ , the lower the temperature at which it occurs. These features point to a smooth evolution in disorder among these samples. As we will see below, however, identifying this disorder is not trivial.

We measured the temperature dependence of resistivity and Hall constant  $R_H$ , of all samples. Carrier density was determined using  $n = 1/R_H e$  ( $e$  is the elementary charge). This single-band expression is justified by the fact that the minimum of the conduction band is at the center of the Brillouin zone [1]. The room temperature values are given in table I.

Mobile electrons can also conduct heat. In general, the measured thermal conductivity has two contributions:  $\kappa_{meas.} = \kappa_{ph} + \kappa_e$ . The latter is the electronic contribution to thermal conductivity which can be estimated using the electric resistivity and the Wiedemann Franz law:  $\kappa_e = L_0 T / \rho$ , where  $L_0 = 2.45 \times 10^{-8} \text{ V}^2/\text{K}^2$  is the Sommerfeld value. Even in the most metallic-like sample,  $\kappa_e \ll \kappa_{meas.}$ . Indeed, for  $\rho \approx 2m\Omega\text{cm}$ , one expects  $\kappa_e/T=L_0/\rho \approx 10^{-3} \text{ W.K}^{-2}\text{m}^{-1}$ . Even at room temperature, this is a tiny fraction of the measured signal. We can therefore safely conclude that  $\kappa_{meas.} \approx \kappa_{ph}$ .

The effective phonon mean free path  $\ell_{ph}$  can be estimated using the kinetic equation,  $\kappa = 1/3 C_{ph} v_s \ell_{ph}$ . Fig.2c shows the temperature dependence of the effective phonon mean free path  $\ell_{ph}$  extracted from our thermal conductivity data, the reported specific heat [22, 23]), and the estimated sound velocity  $v_s = 4.4 \text{ km/s}$ [24]. The smooth evolution of  $\ell_{ph}(T)$  (Fig.2c) is reminiscent of the way thermal conductivity of an insulator evolves upon controlled introduction of disorder, such as NaCl crystals with Ag colloids [25]. Surprisingly, however, the smooth evolution of  $\ell_{ph}(T)$  is not correlated with the electrical properties. As an example, the sample showing the longest  $\ell_{ph}$  (#6) and the one showing the shortest (the as-grown sample, #1) are only slightly different from the charge transport viewpoint. The room temperature carrier density in #6 is five times larger than in #1. How can then the phonon mean free path in #6 be a hundred times longer, in spite of having a higher concentration of scattering centers?

The behavior seen here is to be contrasted with the case of doped semi-conductors such as silicon and germanium [26] or doped oxides such as  $\text{SrTi}_{1-x}\text{Nb}_x\text{O}_3$  [14], where the introduction of Nb dopants leads to a steady enhancement in electrical conductivity (because of the introduction of mobile electrons) and a steady decrease in thermal conductivity (because of a rise in the number of the scattering centers).

Our observation implies that the case of  $\text{In}_2\text{O}_3$  is more complicated and disorder length scale is not simply the interdopant distance. In the as-grown sample #1, the de-

viation from the intrinsic regime starts below 150 K (see Fig.2c). The typical wavelength of an acoustic phonon at this temperature is  $\lambda_{ph}(150 \text{ K}) = \frac{h v_s}{k_B T} = 1.4 \text{ nm}$ . On the other hand, in sample #2, the deviation starts at 30 K, when the phonon wavelength is  $\lambda_{ph}(30 \text{ K}) = 7 \text{ nm}$ . These numbers set the lower boundary to the size of scattering centers. The most prominent candidate for playing this role are clusters of oxygen vacancies which manifest themselves as In particles. They are formed during melt growth in the cooling crystal and have been identified in a recent study combining electron microscopy, light scattering techniques and optical absorption spectroscopy [27]. The concentration of these clusters, which can be as large as several tens of nanometers diminishes upon annealing. This type of extended disorder is the most plausible candidate for scattering long wave-length acoustic phonons in low- $\kappa$  samples.

The two samples with highest  $\kappa_{peak}$  were annealed in the presence of  $\text{H}_2$  (See Table I). Hydrogen is a possible dopant and a shallow donor impurity [28]. H atoms can replace O atoms at their site [29]. The small size of H dopants may allow the survival of high phonon thermal conductivity (which requires small disorder) despite finite electric conductivity (which requires atomic substitution). Note, however, that according to first-principle calculations [30], hydrogen may also occupy interstitial positions and form complexes with indium vacancies. More extensive studies are required to pin down the origin of the link between annealing conditions and peak thermal conductivity.

In the most heat conducting sample (#6), the phonon-mean-free-path  $\ell_{ph}(T)$  becomes as long as 0.3 mm below 10 K, only slightly shorter than the sample thickness (0.5 mm). This means that phonons are close to ballistic. Tantalizingly,  $\ell_{ph}$  peaks at 10 K, which may be a signature of phonon hydrodynamics [31]. In a handful of solids [14, 31–33], the temperature dependence of the phonon mean-free-path displays a local maximum followed by a local minimum. This has been attributed to a regime, first identified by Gurzhi [34], where normal scattering among phonons prevails over both ballistic scattering and Umklapp scattering leading to the so-called Poiseuille flow [31]. It is too early, however, to conclude at this stage that the peak in  $\ell_{ph}(T)$  is a Poiseuille peak. No clear Knudsen minimum is visible down to 5 K. Moreover, the thermal conductivity of the best sample may also be affected by extended disorder, since the phonon wavelength at 10 K is still 'only' 30 nm long. This peak is absent in sample #5, where  $\ell_{ph}$  falls well below the crystal thickness. Note that above 100 K,  $\ell_{ph}$  of all samples merge and approach towards a  $T^{-1}$  behavior. At room temperature,  $\ell_{ph}$  becomes as short as 4 nm, still four times longer than the very long lattice parameter. We will come back to this intrinsic regime below.

Fig.3 compares the thermal conductivity of the best  $\text{In}_2\text{O}_3$  sample (#6) with a selection of other insulators. In all,  $\kappa$  peaks at an intermediate temperature. The peak observed in  $\text{In}_2\text{O}_3$  ( $5,000 \text{ WK}^{-1}\text{m}^{-1}$  at 20 K) is smaller

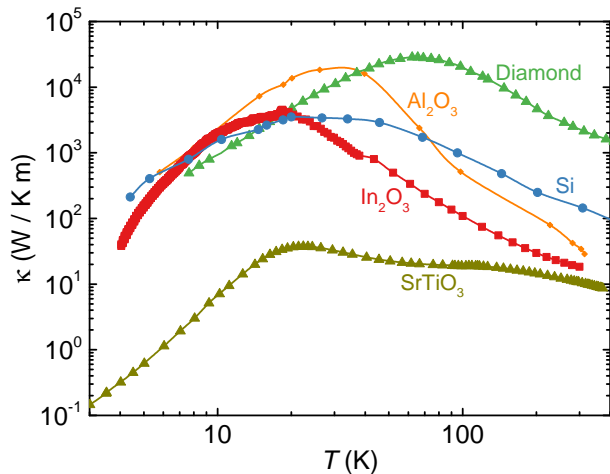


FIG. 3. **Comparison with other solids.** Comparison of the thermal conductivity in the best  $\text{In}_2\text{O}_3$  sample with diamond [12], silicon [35],  $\text{Al}_2\text{O}_3$  (sapphire) [13], and a perovskite  $\text{SrTiO}_3$  [14]. Thermal conductivity in  $\text{In}_2\text{O}_3$  is comparable to a ternary oxide such as  $\text{SrTiO}_3$  at room temperature, but peaks to a value comparable to silicon's peak at low temperature.

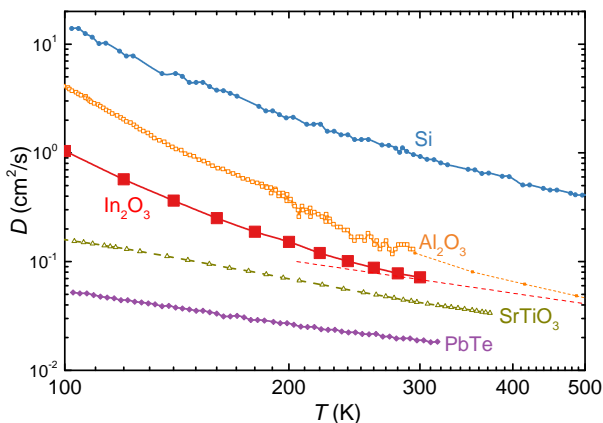


FIG. 4. **Thermal diffusivity in the intrinsic regime:** (a) Temperature dependence of thermal diffusivity,  $D$  in  $\text{In}_2\text{O}_3$ , compared to a few representative solids (Si,  $\text{SrTiO}_3$ ,  $\text{PbTe}$ ) [14] and  $\text{Al}_2\text{O}_3$  [13, 36]. The dashed line represents  $T^{-1}$ . At room temperature,  $D$  in  $\text{In}_2\text{O}_3$  (as well as in  $\text{Al}_2\text{O}_3$  and in Si) approaches this behavior without fully attaining it.

than what is reported in diamond ( $30,000 \text{ WK}^{-1}\text{m}^{-1}$  at 60 K) [12] and in sapphire [13] and slightly exceeds the peak in silicon [35]. Remarkably, the crystal structure of  $\text{In}_2\text{O}_3$  is quite distinct from either the diamond structure or the  $\alpha\text{-Al}_2\text{O}_3$  structure. It has two non-equivalent sites for indium atoms [1, 2]. An indium atom is surrounded by oxygen atoms either in an octahedral coordination or in a trigonal prismatic coordination. In both cases, indium has six immediate oxygen neighbors. In the octahedral coordination all these O atoms are equidistant from the

In atom. In the trigonal prismatic coordination, however, there is a slight difference in distance between three pairs of O atoms. Each oxygen atom is surrounded by one indium atom of the first type and three indium atom of the second type [37].

Thus, the octahedral coordination is present in both sapphire and indium oxide, two binary compounds with remarkably large low-temperature thermal conductivity. We note that other insulators such as  $\text{Tl}_2\text{O}_3$  [38] crystallize in cubic bixbyite structure, but their thermal conductivity remains unexplored. Let us also note that in  $\beta\text{-Ga}_2\text{O}_3$ ,  $\kappa$  peaks to  $560 \text{ WK}^{-1}\text{m}^{-1}$  [39]. This is to be contrasted with ternary oxides, such as perovskites [40], where  $\kappa_{peak}$  is in the range of  $40 \text{ WK}^{-1}\text{m}^{-1}$ , two orders of magnitude smaller than the two binary oxides of Fig. 3. As seen in the figure, and discussed in more detail below, this difference disappears at room temperature.

Let us now turn our attention to the magnitude of thermal diffusivity in the intrinsic regime. Above 100 K, thermal conductivity in all six samples becomes identical in magnitude and in temperature dependence. Heat conduction in this temperature range is governed by phonon-phonon scattering. Our data combined with specific heat reported previously [22], allows us to extract the thermal diffusivity ( $D = \frac{\kappa}{c'}$ , where  $c'$  is the specific heat per volume). As seen in Fig. 4,  $D$  evolves faster than  $T^{-1}$  below 250 K, but becomes close to the expected  $T^{-1}$  behavior near room temperature. The figure compares  $\text{In}_2\text{O}_3$  with a few other solids. The room-temperature thermal diffusivity of  $\text{In}_2\text{O}_3$  is only  $7 \text{ mm}^2\text{s}^{-1}$ . This is more than one order of magnitude lower than Si ( $D \approx 90 \text{ mm}^2\text{s}^{-1}$ ), but close to what has been observed in  $\text{SrTiO}_3$  ( $D \approx 4 \text{ mm}^2\text{s}^{-1}$ ) [14] and other ternary oxides [36, 41] including cuprates [17].

In this intrinsic regime, the asymptotic  $T^{-1}$  temperature dependence of thermal diffusivity represents the temperature dependence of the phonon-phonon scattering cross section. Recently, an empirical lower boundary to  $D$  in this regime was noticed [14, 15]. Expressing thermal diffusivity,  $D$ , as a function of the Planckian time,  $\tau_P = \hbar/k_B T$  one can write:

$$D = s v_s^2 \tau_P \quad (1)$$

Here,  $s$  is a dimensionless parameter (representing the ratio of the scattering time  $\tau$  to  $\tau_P$ ). It was observed [15] that  $s$  does not fall below unity in any known solid. According to our data  $s \approx 14$  in  $\text{In}_2\text{O}_3$  at room temperature. Note that since  $D$  is still evolving faster than  $T^{-1}$  below 300 K, our data can only put an upper boundary to  $s$ . In the case of  $\text{Al}_2\text{O}_3$ , data above room-temperature [36] reduces  $s$ , since the slope of the  $T^{-1}$  thermal diffusivity evolves between 300 K and 1200 K. Thus,  $\text{In}_2\text{O}_3$ , in spite of being an excellent conductor of heat at low temperatures, emerges more akin to low-diffusivity oxides [14, 17, 41].

A recent theoretical account of the empirical boundary to thermal diffusivity [14, 15, 17] was put forward by Mousatov and Hartnoll [16], who argued that the



perature of  $T_M = 2223$  K [9], an interatomic distance of  $a = 0.21$  nm [2], and a sound velocity of  $v_s = 4.4$  km/s [24]. As a result, one finds  $v_M/v_s \approx 15$ . Our room-temperature data sets an upper bound to  $\tau/\tau_P \leq 15$ . As seen in Fig. 5, these numbers put  $\text{In}_2\text{O}_3$  inside the green stripe in company of numerous other oxides and ionic salts.

Interestingly,  $\text{In}_2\text{O}_3$  and  $\text{Al}_2\text{O}_3$  reside at the opposite ends of the green stripe. This is understandable. Mousatov and Hartnoll [16] already noticed that what puts two alkali halides (LiF and RbI) with identical crystal structures (and comparable room-temperature thermal conductivities) far way in this plot is the difference in the atomic masses. Given that the atomic mass of In (114) is about four time larger than Al (28), the same can be said about  $\text{In}_2\text{O}_3$  and  $\text{Al}_2\text{O}_3$ . In both cases, heaviness reduces the sound velocity [42] and lightness promotes zero-point motion and proximity to the Planckian boundary [16].

In summary, we measured the thermal conductivity of the transparent semiconductor  $\text{In}_2\text{O}_3$  and found a peak

at 20 K whose amplitude is surpassed only by a few solids. The peak thermal conductivity was found to be extremely sensitive to disorder. In the intrinsic regime, thermal diffusivity respects a boundary found in other insulators.

We thank Sean Hartnoll and Kostya Trachenko for discussions and Detlef Klimm for a critical reading of the manuscript. This work was supported in France by the Agence Nationale de la Recherche (ANR-18-CE92-0020-01; ANR-19-CE30-0014-04) and by 'Jeunes Equipes de l'Institut de Physique du Collège de France'. It was partly performed in the framework of GraFOx, a Leibniz-Science Campus partially funded by the Leibniz Association Germany. It was also supported by the National Key Research and Development Program of China (Grant no. 2016YFA0401704), the National Science Foundation of China (Grants No. 51861135104 and No. 11574097) and Fundamental Research Funds for the Central Universities (Grant no. 2019kfyXMBZ071). L. X. acknowledges a PhD scholarship by the China Scholarship Council (CSC).

- 
- [1] O. Bierwagen, *Semiconductor Science and Technology* **30**, 024001 (2015).
- [2] S. Z. Karazhanov, P. Ravindran, P. Vajeeston, A. Ulyashin, T. G. Finstad, and H. Fjellvåg, *Phys. Rev. B* **76**, 075129 (2007).
- [3] A. Walsh and C. R. A. Catlow, *J. Mater. Chem.* **20**, 10438 (2010).
- [4] M. Steiner and A. Kapitulnik, *Physica C: Superconductivity* **422**, 16 (2005).
- [5] A. Kapitulnik, S. A. Kivelson, and B. Spivak, *Rev. Mod. Phys.* **91**, 011002 (2019).
- [6] M. Ovia, B. Sacépé, and D. Shahar, *Phys. Rev. Lett.* **102**, 176802 (2009).
- [7] K. Makise, N. Kokubo, S. Takada, T. Yamaguti, S. Ogura, K. Yamada, B. Shinozaki, K. Yano, K. Inoue, and H. Nakamura, *Science and Technology of Advanced Materials* **9**, 044208 (2008).
- [8] D. R. Hagleitner, M. Menhart, P. Jacobson, S. Blomberg, K. Schulte, E. Lundgren, M. Kubicek, J. Fleig, F. Kubel, C. Puls, A. Limbeck, H. Hutter, L. A. Boatner, M. Schmid, and U. Diebold, *Phys. Rev. B* **85**, 115441 (2012).
- [9] Z. Galazka, R. Uecker, K. Irmscher, D. Schulz, D. Klimm, M. Albrecht, M. Pietsch, S. Ganschow, A. Kwasniewski, and R. Fornari, *Journal of Crystal Growth* **362**, 349 (2013).
- [10] T. Ashida, A. Miyamura, N. Oka, Y. Sato, T. Yagi, N. Taketoshi, T. Baba, and Y. Shigesato, *Journal of Applied Physics* **105**, 073709 (2009).
- [11] D. G. Onn, A. Witek, Y. Z. Qiu, T. R. Anthony, and W. F. Banholzer, *Phys. Rev. Lett.* **68**, 2806 (1992).
- [12] A. V. Inyushkin, A. N. Taldenkov, V. G. Ralchenko, A. P. Bolshakov, A. V. Koliadin, and A. N. Katruscha, *Phys. Rev. B* **97**, 144305 (2018).
- [13] D. G. Cahill and R. O. Pohl, *Annual Review of Physical Chemistry* **39**, 93 (1988).
- [14] V. Martelli, J. L. Jiménez, M. Continentino, E. Baggio-Saitovitch, and K. Behnia, *Phys. Rev. Lett.* **120**, 125901 (2018).
- [15] K. Behnia and A. Kapitulnik, *Journal of Physics: Condensed Matter* **31**, 405702 (2019).
- [16] C. H. Mousatov and S. A. Hartnoll, *Nature Physics* **16**, 579584 (2020).
- [17] J. Zhang, E. D. Kountz, K. Behnia, and A. Kapitulnik, *Proceedings of the National Academy of Sciences* **116**, 19869 (2019).
- [18] E. Tulipman and E. Berg, arXiv:2004.03617 (2020).
- [19] Z. Galazka, R. Uecker, and R. Fornari, *Journal of Crystal Growth* **388**, 61 (2014).
- [20] Z. Galazka, *Transparent Semiconducting Oxides Bulk Crystal Growth and Fundamental Properties* (Jenny Stanford Publishing, 2020).
- [21] L. Xu, X. Li, X. Lu, C. Collignon, H. Fu, J. Koo, B. Fauqué, B. Yan, Z. Zhu, and K. Behnia, **6** (2020), 10.1126/sciadv.aaz3522.
- [22] E. Cordfunke and E. Westrum, *Journal of Physics and Chemistry of Solids* **53**, 361 (1992).
- [23] K. Bachmann, F. Hsu, and J. Remeika, *Physica Status Solidi. A, Applied Research* **67**, K39 (1981).
- [24] N. Preissler, O. Bierwagen, A. T. Ramu, and J. S. Speck, *Phys. Rev. B* **88**, 085305 (2013).
- [25] J. W. Vandersande and C. Wood, *Contemporary Physics* **27**, 117 (1986).
- [26] J. Carruthers, T. Geballe, H. Rosenberg, and J. M. Ziman, *Proceedings of the Royal Society of London. Series A. Mathematical and Physical Sciences* **238**, 502 (1957).
- [27] M. Albrecht, R. Schewski, K. Irmscher, Z. Galazka, T. Markurt, M. Naumann, T. Schulz, R. Uecker, R. Fornari, S. Meuret, and M. Kociak, *Journal of Applied Physics* **115**, 053504 (2014).
- [28] S. Limpijumngong, P. Reunchan, A. Janotti, and C. G. Van de Walle, *Phys. Rev. B* **80**, 193202 (2009).
- [29] Z. Galazka, K. Irmscher, M. Pietsch, T. Schulz, R. Uecker, D. Klimm, and R. Fornari, *CrystEngComm*

- 15**, 2220 (2013).
- [30] J. B. Varley, H. Peelaers, A. Janotti, and C. G. V. de Walle, *Journal of Physics: Condensed Matter* **23**, 334212 (2011).
- [31] H. Beck, P. F. Meier, and A. Thellung, *Phys. stat. sol. (a)* **24**, 11 (1974).
- [32] Y. Machida, A. Subedi, K. Akiba, A. Miyake, M. Tokunaga, Y. Akahama, K. Izawa, and K. Behnia, *Science Advances* **4**, eaat3374 (2018).
- [33] Y. Machida, N. Matsumoto, T. Isono, and K. Behnia, *Science* **367**, 309 (2020).
- [34] R. N. Gurzhi, *Soviet Physics Uspekhi* **11**, 255 (1968).
- [35] C. J. Glassbrenner and G. A. Slack, *Phys. Rev.* **134**, A1058 (1964).
- [36] A. M. Hofmeister, *Physics and Chemistry of Minerals* **41**, 361 (2014).
- [37] P. Reunchan, X. Zhou, S. Limpijumnong, A. Janotti, and C. G. Van de Walle, *Current Applied Physics* **11**, S296 (2011).
- [38] P.-A. Glans, T. Learmonth, K. E. Smith, J. Guo, A. Walsh, G. W. Watson, F. Terzi, and R. G. Egdell, *Phys. Rev. B* **71**, 235109 (2005).
- [39] M. Handweg, R. Mitdank, Z. Galazka, and S. F. Fischer, *Semiconductor Science and Technology* **30**, 024006 (2015).
- [40] M. Tachibana, T. Kolodiazny, and E. Takayama-Muromachi, *Applied Physics Letters* **93**, 092902 (2008).
- [41] A. M. Hofmeister, *Journal of Applied Physics* **107**, 103532 (2010).
- [42] K. Trachenko, B. Monserrat, C. J. Pickard, and V. V. Brazhkin, arXiv:2004.04818 (2020).
- [43] L. Lindsay and D. A. Broido, *Journal of Physics: Condensed Matter* **20**, 165209 (2008).
- [44] G. Grimvall and S. Sjödin, *Physica Scripta* **10**, 340 (1974).
- [45] D. C. Wallace, *Proceedings of the Royal Society of London. Series A: Mathematical and Physical Sciences* **433**, 631 (1991).